Materials Characterization 190 (2022) 112059

Contents lists available at ScienceDirect

Materials Characterization

journal homepage: www.elsevier.com/locate/matchar

Effect of high-pressure torsion on high cycle fatigue of commercially pure Cu: Some insights from formation of surface micro-cracks

Shobhit P. Singh [a], Ajay Rijal [a], Thomas Straub [b], Jae-Kyung Han [c], Tobias Kennerknecht [b], Christoph Eberl [b], Megumi Kawasaki [c], Praveen Kumar [a,*]

[a] Department of Materials Engineering, Indian Institute of Science, Bangalore 560012, India
[b] Fraunhofer Institute for Mechanics of Materials (IWM), 79108 Freiburg im Breisgau, Germany
[c] School of Mechanical, Industrial, and Manufacturing Engineering, Oregon State University, Corvallis, OR 97331, USA

ARTICLE INFO

Keywords:
High-pressure torsion
Commercially pure Cu
Bending fatigue
Surface micro-cracks
Ultra-fine grains

ABSTRACT

In most technical applications, fatigue is related to highly localized load distributions. While high-pressure torsion (HPT) materials cannot prevent crack initiation, they promise to improve the resistance to crack nucleation and propagation. Herein, commercially pure Cu was processed through HPT at a pressure of 6 GPa up to 50 turns. Small "cantilever" type samples were fabricated from annealed and HPT samples. The cantilever samples were subjected to fully-reversed cyclic bending. The maximum stress amplitude was chosen to reach the high cycle fatigue regime, and the experiments were stopped when the resonant frequency decayed by 20%. Compared to the annealed samples, the HPT samples showed higher lifetimes. The grain size in the HPT samples remained stable during fatigue, and dislocation substructures, a stacking of parallel dislocations, could be observed in all samples. In HPT samples, the area fraction of surface micro-cracks increased with the local stress amplitude. This can be attributed to the inhibition of crack nucleation at low stresses due to the high strength of HPT samples and the crack arrest at the boundaries of their ultra-fine grains. The obtained insights into the microstructure-fatigue response relationship are vital for understanding the initial stages of fatigue failure in ultra-fine-grained materials and their technological adoption for applications in extreme environments.

1. Introduction

Over the past three decades, severe plastic deformation (SPD) has been widely investigated and applied for fabricating ultrafine-grained (UFG) materials [1–5]. These UFG materials often show high strength at room temperature due to the grain boundary strengthening (i.e., Hall-Petch relationship) and high ductility at moderately high temperatures due to the onset of superplasticity. Although a few studies have shown that SPD processing may lead to a simultaneous increase in both the strength and the ductility [6–10], these materials often show poor ductility at low temperatures. This manifestation of the strength-ductility paradox, i.e., mechanical processing leads to an increase in either strength or ductility and seldom both [6], has an interesting implication on the room temperature fatigue life of SPD processed UFG materials: They have superior fatigue resistance as compared to the coarse-grained (CG) materials in the high cycle fatigue (HCF) regime due to their higher strength; however, they show inferior resistance to the low cycle fatigue (LCF) due to the poor ductility [11–15].[1] In practice, a heat treatment that may enhance the ductility and minimize the microstructural instabilities under cyclic loading, such as short-term annealing resulting in lowering of the grain boundary energy and formation of bimodal grain size distribution [10], may enhance the LCF life of the SPD processed UFG materials [12,16]. Besides short-term annealing, microstructural instabilities, such as dynamic grain growth, recrystallization, etc., in the SPD-processed UFG materials occurring during the cyclic loading, which may induce cyclic softening and significant shear banding that are often considered detrimental to fatigue life, may also be minimized by lowering the purity of the material [15] and alloying [12,17]. Hence, a low purity metal, such as commercially pure (CP) Cu (instead of high purity Cu) [15], may be better suited for directly comparing the fatigue response of the annealed coarse-grained (CG) and SPD processed UFG materials. On the other hand, grain growth

* Corresponding author.
E-mail address: praveenk@iisc.ac.in (P. Kumar).

[1] Similar to the coarse grain materials, the UFG materials also follow the classic Basquin and Coffin-Manson laws in the HCF and LCF regimes, respectively, however, with different coefficients and, possibly, exponents [12,15,44].

https://doi.org/10.1016/j.matchar.2022.112059
Received 17 March 2022; Received in revised form 16 May 2022; Accepted 12 June 2022
Available online 16 June 2022
1044-5803/© 2022 Elsevier Inc. All rights reserved.

in UFG materials has often been reported in high purity UFG materials subjected to cyclic loading [18–21].

Commercially pure Cu is an excellent electrical conductor; however, it has relatively poor mechanical strength. This sub-optimal "strength-conductivity" combination limits its application in the high demanding electrical transmission and connector applications. However, processing of CP Cu by high-pressure torsion (HPT) to high strains (e.g., $\geq$ 200) results in a remarkable increase in the strength ($\geq$ 300%), without a significant loss in the electrical conductivity ($\leq$ 30%). Moreover, these properties remain stable during prolonged storage under ambient condition, i.e., natural aging [22–25]. It should be noted that HPT is one of the severe plastic deformation (SPD) methods that is quite effective in imposing very high plastic strains into the sample in a short time [1]. In this context, examination of the fatigue life of HPT-processed CP Cu, therefore, may further provide important information about the structural reliability of the SPD-processed UFG Cu for long-term applications. Interestingly, the fatigue response of the SPD-processed UFG Cu has been studied in both low and high cycle fatigue regimes [12–15]; however, similar studies on HPT-processed Cu are rather limited [15]. In practice, the HPT-processed material exhibited longer HCF life as compared to CG material as well as UFG Cu fabricated using equal-channel angular pressing (ECAP) [15], which is another widely used SPD process [4]. However, the HPT samples were noted to be susceptible to an increased crack propagation once the crack was nucleated. Significant shear banding occurs in these samples, which often become the preferred sites for crack nucleation. However, microstructural examination focusing on the evolution of dislocation substructure and the distribution of the surface cracks during the initial stages of fatigue of HPT Cu is limited. Since the time taken for the initial stages of the damage accumulation accounts for the significant fraction of the HCF life, understanding the effect of HPT on the above is quite important.

Accordingly, this study aims to examine, in a high throughput fashion, the effects of HPT on the distribution of the surface cracks as a function of stress and the formation of dislocation substructure in the CP Cu during the initial stages of the fatigue damage in the HCF regime. While similar dislocation substructures formed in both the CG and the HPT samples, the distribution of surface cracks and the number of cycles required to damage the samples by the same ratio were significantly different in these two kinds of samples. A qualitative relationship between applied stress amplitude, grain size and distribution of surface cracks is established to understand the initiation of fatigue damages in CP Cu.

2. Experimental material and procedure

Electrical grade CP Cu was machined into disks of 10 mm diameter and 1 mm thickness, which were then isothermally annealed at 600 °C for 1 h for homogenizing the microstructure and removing the residual stresses induced during machining. Subsequently, a few of the disks were thinned down to a final thickness of 0.85 mm by metallographic polishing and processed through quasi-constrained HPT [26] for 50 turns at room temperature while applying a pressure of 6 GPa.

Samples for fatigue tests were fabricated from both the annealed (i.e., coarse-grained) and the HPT processed Cu samples.[2] Samples of specific dimensions, having a gauge length of 0.8 mm (see Fig. 1a), were machined using micro-electrical discharge machining (μ-EDM). The sides of the samples were machined with a gradually decreasing feed-rate, so that a smooth surface (roughness, $R_z \sim 2$ μm) could be obtained. Following μ-EDM, both the flat faces of the samples were metallographically polished down to 40 nm colloidal silica. Following metallographic polishing, the thickness of the annealed CG and the HPT samples were approximately 1 mm and 240 μm, respectively. Although the equivalent strain, ε_{eq}, imposed by HPT varies linearly with the distance away from the center of the disk, r (i.e., $\varepsilon_{eq} \sim r$) [1], the effect of HPT strain on the microstructure (e.g., grain size, misorientation, etc.) and properties of the CP Cu often saturate beyond a few tens of strain [23]. Here, the average HPT strain in the gauge section of the fatigue sample was ~400 and hence the microstructure of the entire sample can be assumed to be homogeneous, with an average grain size of ~300 nm. The average grain size of annealed CG samples was ~11 μm. Hence, there would be approximately 800 and 90 grains across the thickness of HPT and annealed samples, respectively. Details of microstructural and hardness analysis, along with the stability under room temperature aging, of the HPT Cu samples are available in references [22,23].

Fatigue tests were performed using a custom-designed resonant fatigue setup. The details of the test setup are available in [27], and here some of the salient features of its working principles are described with the help of the schematic illustrated in Fig. 1b. One of the ends of the fabricated "cantilever" sample was affixed to the "rigid" structure of the setup via a spring, and this end was then pushed to-and-fro in the out-of-plane direction by a piezo-actuator at the resonant frequency of the sample. The resonant frequency of the samples, depending on their dimensions and mass attached at the bottom (see Fig. 1b), varied between 385 and 450 Hz. The piezo-actuator applied a deflection amplitude near the bottom-end of the spring (where it is attached to the sample – see Fig. 1b) that corresponded to a desired maximum stress amplitude, $\sigma_{a,max}$, at the top-end of the gauge length (i.e., at the beginning of the shoulder section) of the sample (see Fig. 1a). Finite element analysis (FEA), using ANSYS® and assuming linear elastic theory, was used to estimate the stress field across the length of the sample for a given deflection: Fig. 1c shows a representative stress distribution, clearly demonstrating that the highest stress was concentrated near the fixed end of the gauge section, however, away from the dove-tail section of the sample. The deflection of the free-end was continuously monitored using a laser-based measurement system. It should be noted that the stress at a point on the surface of a sample varied linearly with the distance away from the free (or loading) end of the sample, and its value fully reversed during one cycle. Hence, the stress ratio, R, in these tests was −1. Fatigue experiments on HPT samples were performed at $\sigma_{a,\max}$ values of 170, 185 and 200 MPa, and annealed samples were tested at $\sigma_{a,max}$ values of 80, 150 and 172 MPa. Since the yield strength of 50 turns HPT sample was ~500 MPa (based on hardness value [22,23]), and the yield stress of annealed Cu is $\geq$170 MPa at strain rates of $>10^{-3}$ s^{-1} [28,29], the maximum stress amplitudes used here for conducting fatigue tests were below the yield stress.

As the fatigue progresses, it induces the formation of defects in the sample (e.g., surface micro-cracks), resulting in a decrease in its stiffness. With the decrease in the stiffness, the resonant frequency of the sample also decreases. All tests were stopped after a 20% decrease in the resonant frequency, f, was observed (i.e., $\Delta f/f_0 = 0.2$, where f_0 is the initial resonant frequency). A few tests were repeated to examine if the trend varied noticeably; however, here, the data corresponding to the sample registering the highest number of cycles before the above test termination criterion was met are reported. This, therefore, enables discussion based on the most fatigue-resistant sample for a given test condition.

Following a fatigue test, both the flat surfaces of the sample were examined using an optical microscope and a scanning electron microscope (SEM). To gain further insights into the formation of dislocation substructure, which often reveals the vital signatures of the operational fatigue mechanism, a transmission electron microscope (TEM) was used to examine the thin lamellae obtained from a region near the surface micro-cracks in both types of samples. 80–90 nm thick lamellae were fabricated using the focused ion beam (FIB) machining. TEM imaging was performed using Titan Themis 300 kV system (however, it was not aberration-corrected). Since CP Cu is a standard FCC material, the zone axis (ZA) was kept as [101] for obtaining the diffraction pattern so that

[2] HPT samples were stored under ambient conditions for about two months before tests were performed. However, microstructure of 50 turns HPT sample did not evolve during natural aging up to, at least, 21 months [22,23].

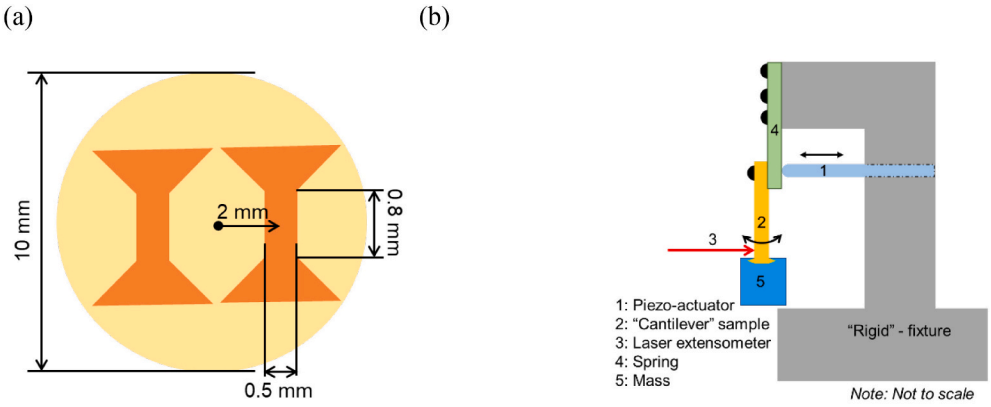

Fig. 1. Schematic illustrations of the (a) "cantilever" fatigue samples, along with the relevant dimensions, fabricated from the annealed and the HPT Cu disks, and (b) experimental setup used to perform fatigue experiments in bending by exciting the "cantilever" sample at its resonance frequency. A mass was attached to the sample to tune the resonant frequency of the sample. The drawing of the setup is adapted from reference [27]. (c) Representative distribution of bending (normal) stress, as obtained using FEA, in a sample during a bending fatigue test.

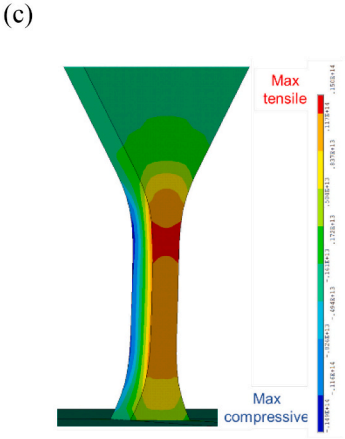

the sample maneuvering for dislocation imaging could become easier. The samples were then tilted to a particular direction according to the ***g***. ***b*** = 0 criterion, where **g** and **b** are reciprocal ZA vector and Burgers vector, respectively, for imaging dislocations in a grain.

3. Results and discussion

Fig. 2a shows the number of cycles, *N*, required to reduce the resonant frequency of annealed and HPT Cu samples by 20% (i.e., $\Delta f/f_0 = 0.2$) for a given maximum stress amplitude, $\sigma_{a,max}$. Since the major fraction of the high cycle fatigue (HCF) life is spent in the crack nucleation and Stage I growth of the micro-cracks, the trend shown by the variation of above calculated *N* as a function of $\sigma_{a,max}$ may reasonably represent the fatigue life of the material. The "S-N" curve shown in Fig. 2a readily reveals that the fatigue response of both types of samples under the applied test conditions lay in the HCF regime, which is consistent with the assumption that the global stresses in the sample did not exceed the yield strength of both types of samples. Furthermore, Fig. 2a suggests that the HPT samples could be more fatigue resistant than the annealed CG samples (e.g., for $\sigma_{a,max}$ of ~170 MPa, number of

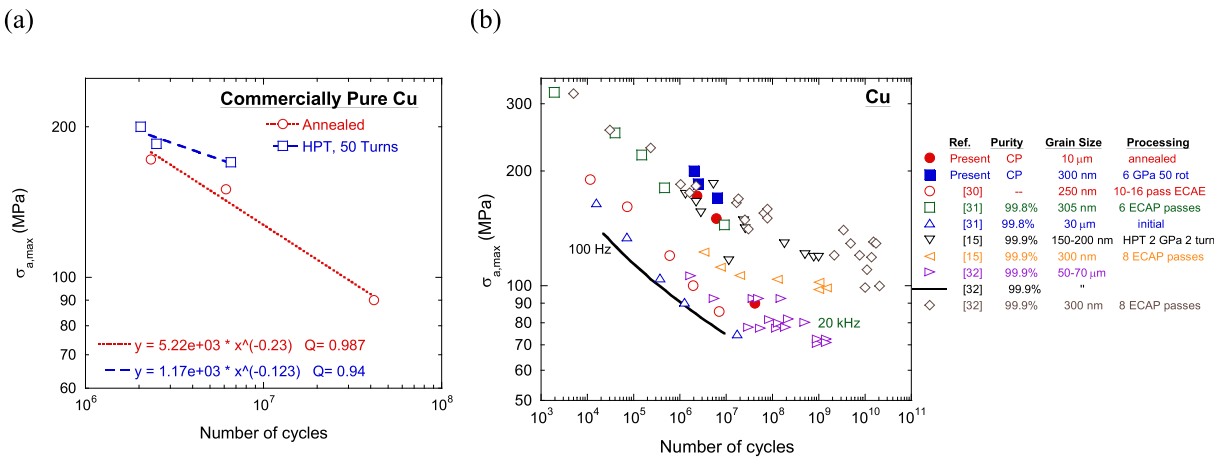

Fig. 2. (a) An "S-N" type plot showing the effect of maximum stress amplitude, $\sigma_{a,max}$, on the number of cycles taken to failure (i.e., $\Delta f/f = 20\%$) for the annealed CG and the HPT processed UFG Cu samples. The broken lines are the best curve-fits, using the Basquin equation (which is given in the legend, along with the value of the regression parameter, *Q*, for both the types of samples), and (b) a plot comparing the fatigue life of commercially pure Cu reported in this study with the literature on the relatively pure Cu. The data shown in (b) is taken from [15,30–32].

cycles to "failure" for HPT and CG samples were 6.6×10^6 and 2.3×10^6, respectively). It also suggests an improvement in the fatigue life due to the HPT processing would be quite pronounced at lower $\sigma_{a,max}$. The apparent higher HCF life for SPD processed UFG materials is consistent with previous reports [12,15] as shown in Fig. 2b, which compares the fatigue life of Cu obtained in the present study and earlier studies on CG and UFG Cu of low purity. The trend reported in the earlier studies, when examined individually, reveals an increased fatigue life of UFG Cu as compared to the CG Cu. Although differences in the definition of fatigue failure (e.g., a decay in the resonant frequency by 20% in this study while complete fracture of samples in a few other studies) and the wide scatter associated with the fatigue life data of Cu, as shown in Fig. 2b, restrict quantification and direct comparison, the overall trend obtained in this study using fewer samples and lesser number of tests confirms high throughput nature and efficacy of the "cantilever" fatigue bending test methodology. In practice, the plots shown in Fig. 2 provide a simplistic and qualitative way of comparing the data obtained from the above-defined fatigue life (i.e., drop in resonant frequency by a certain fraction) with the previously published data.

Figs. 3a-c show a few representative optical micrographs revealing the formation of micro-cracks on the surfaces of the HPT samples at $\sigma_{a,max}$ of 170, 185 and 200 MPa, respectively. Since several micro-cracks originated away from the edges of the samples (e.g., the center of the flat faces of the samples), the design and fabrication of the test samples can be considered to inhibit the formation of pre-existing stress concentrators associated with sample machining (e.g., the sharp edges, chamfers, etc.). The insets in these micrographs show a few micro-cracks at higher magnification(s). Significant shear banding can be observed in the vicinity of the micro-cracks. Furthermore, several small micro-cracks are also evident in the shear bands (see inset showing the highest magnification micrograph in Fig. 3a), which might coalesce to form a longer micro-crack. These clearly highlight the important role of shear bands in the nucleation of micro-cracks in these samples during cyclic loading.

As shown in Figs. 3a-c, the spread of the shear-banding and plasticity-affected region in the vicinity of the micro-cracks spread to a region much larger than grain size (i.e., ~300 nm). This might be attributed to the agglomeration of similarly oriented grains (with a little in-plane misorientation between them). Although the HPT sample did not show an overall preference for a crystallographic texture, groups of grains of similar orientation were often observed together (see Fig. 4). Such groupings may induce the spread of plasticity in the neighboring grains from the favorably oriented grain that might have formed a surface micro-crack at first.

Figs. 3a-c also reveal that the area fraction of the surface micro-cracks in each test condition was higher near the fixed end, where the stress amplitudes were the highest. Further, a comparison of Fig. 3a-c indicates that as $\sigma_{a,max}$ in these "cantilever" samples was increased, the extent of the region filled with discernable surface micro-cracks also increased. Interestingly, a close inspection of Figs. 3a-c reveals that the area fraction of the surface micro-cracks gradually decreased away from the fixed end (i.e., as the stress amplitude decreased); however, the micro-cracks ceased to form beyond a certain distance from the fixed end, suggesting a presence of the threshold of the stress amplitude, σ_a, where the region below this value did not form the surface cracks in the HPT samples.

To gain some quantitative insights into the effect of σ_a on the micro-crack formation, the variation of the area fraction of micro-crack region was plotted as a function of σ_a (see Fig. 3d). The value of σ_a on the surface of the sample corresponds to its undamaged state (which was determined using FEA, assuming linear elasticity). The area fraction of the region with surface micro-cracks was measured using ImageJ®, an image analysis software. Here, the gauge section of a sample was divided into numerous small rectangular sections of 100 μm in height and 500 μm in width (i.e., equivalent to the width of the gauge section), and the area fraction of the surface cracks in each section of the sample was calculated by applying the threshold contrast in the ImageJ®. Fig. 3d clearly reveals that, within the scatter of data, the area fraction of the surface micro-cracks decreased with σ_a and negligible micro-cracks formed below a certain σ_a value. It should be noted that all datum points shown in Fig. 3d were obtained from testing only 3 samples, which clearly demonstrates the efficacy of test setup in enhancing the throughput.

For comparison purposes, Fig. 5a and b show a few representative SEM micrographs showing the visible surface cracks in the annealed CG Cu samples after fatigue loading at $\sigma_{a,\max}$ of 80 and ~ 170 MPa, respectively; here, the gauge lengths of the fatigue samples are vertical in the micrographs. In practice, the surface cracks in the CG Cu samples could not be discerned using an optical microscope (i.e., at low magnifications) and hence an SEM was used to obtain relatively higher magnification micrographs for observing surface micro-cracks. Similar to Fig. 3a-c, Fig. 5a and b also show the presence of shear banding and the formation of micro-cracks in their vicinity and hence shear banding was not associated with only UFG samples. However, the overall length and the area fraction of the surface micro-cracks in the annealed CG samples were significantly smaller than those in the HPT samples. This is confirmed by Fig. 5c, which shows the variation of the fraction of the area wherein the surface micro-cracks formed in the annealed CG samples after the fatigue tests as a function of stress amplitude. Although the area fraction of the surface micro-cracks in the annealed samples decreased with σ_a, as was shown in the HPT samples, the values of area fraction in the annealed samples were considerably smaller at the higher stresses (e.g., 160 MPa). However, while the HPT samples did not show noticeable surface cracks at the lower stresses (e.g., $<$ 145 MPa), the annealed samples continued to accumulate surface cracks at significantly lower stress (e.g., up to 120 MPa). Overall, consistent with Fig. 2, the microstructural analysis also indicates that HPT processing suppresses crack nucleation quite effectively in the low-stress regime, resulting in a significantly longer HCF life.

Hence, based on the observations in Figs. 2, 3 and 5, the following three inferences can be extracted: HPT processing leads to (i) enhancement in the HCF life, (ii) inhibition of cracking at low stress amplitudes, and (iii) formation of a significantly large number of the surface micro-cracks at higher stress amplitudes. The last two apparently opposing effects can be explained based on the grain-refining effect of the HPT that strengthens the material. Since all tests were terminated when a fixed reduction in the resonant frequency was observed, one may reasonably assume that a similar fractional reduction in the effective stiffness of the sample must have occurred when the tests were terminated. In other words, the effect of the surface micro-cracks on reducing the effective stiffness (and hence resonant frequency) of all samples, irrespective of the grain sizes, should be equivalent. Accordingly, as only a few micro-cracks were observed in the annealed samples, they must be longer than those observed in the HPT samples to result in a decrease in the stiffness by the same fraction. Hence, the micro-cracks in the HPT processed samples would be confined to near the surface region, which is reasonable as penetrating deeper through several high angle grain boundaries (HAGB)[3] is generally considered less favorable for the fatigue micro-cracks as their growth is plasticity controlled [33]. Hence, as schematically shown in Fig. 6 where the red arrows represent the micro-cracks originating from the surfaces, grain boundaries act as an efficient barrier for these micro-cracks. Due to their inability to grow deeper into the UFG material, a larger number of surface cracks must be formed to result in a consistent change in the stiffness of the sample. Since fatigue life is primarily dependent on the longest of the cracks, the HCF life of the annealed samples would be lower than the HPT samples; this is consistent with the observations in this study as well as a few previous

[3] HPT processed UFG materials often comprise a very high fraction of HAGB, especially if the imposed strain is very high (e.g., ~400 for HPT processed CP Cu) [1,4,22].

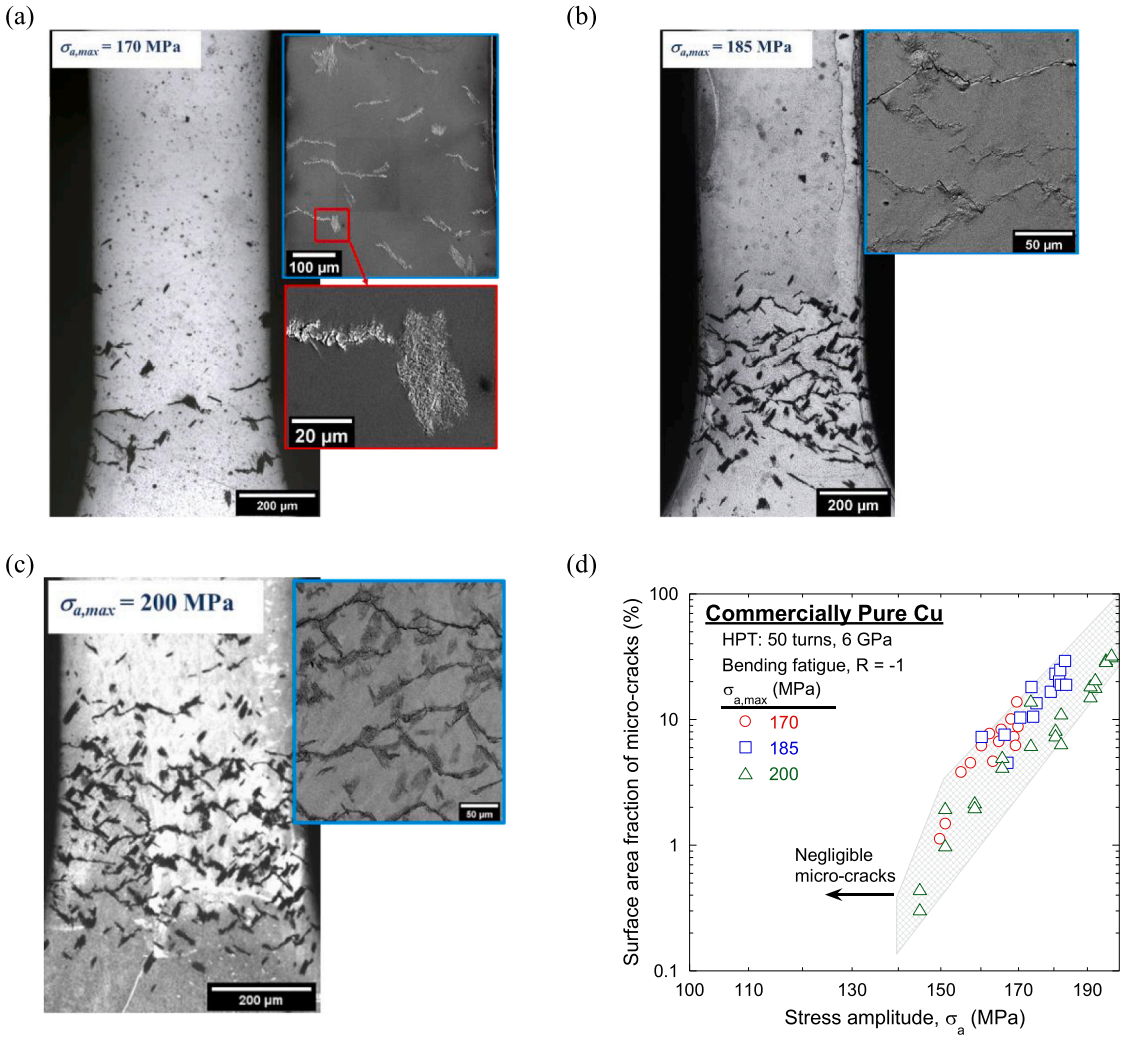

Fig. 3. Optical micrographs of the surface of the HPT Cu samples after the bending fatigue tests: $\sigma_{a,max}$ = (a) 170, (b) 185 and (c) 200 MPa. The fixed end was near the bottom of each micrograph. A few high magnification micrographs obtained using SEM are shown in the inset. (d) Variation of the area fraction of the micro-cracks as a function of σ_a on a log-log scale. Both flat surfaces of each sample were examined, and the area fraction of both sides is averaged. A "band" covering the scatter in the data is shown in (d) to highlight the overall trend.

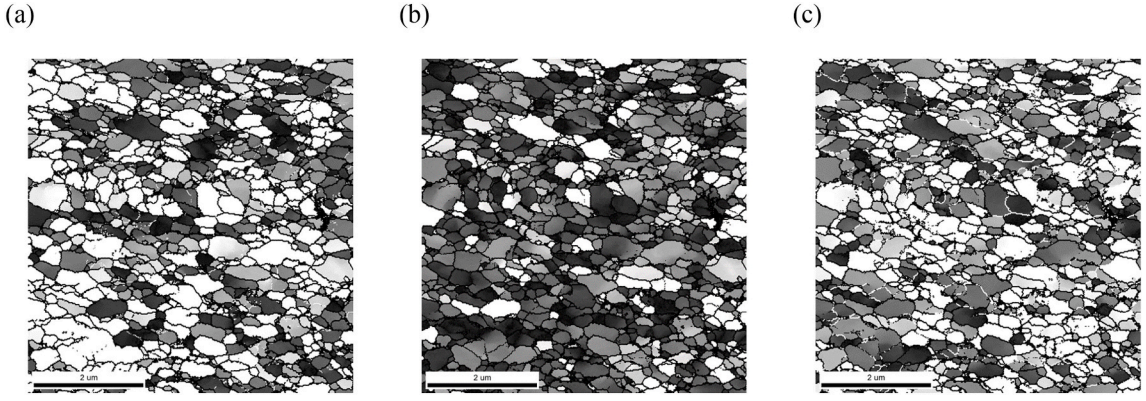

Fig. 4. Electron back-scattered diffraction (EBSD) maps showing the distribution of near (a) (001)-, (b) (101)- and (c) (111)-oriented grains in the sample processed through HPT up to 50 turns. The mentioned orientation is normal to the plane, and the white and dark regions show the maximum and minimum presence of the particular orientation, respectively. The area fraction of near (001), (101) and (111)-oriented grains were approximately 37, 16 and 47%, respectively. The maps shown here are representative of the gauge section of the fatigue samples. The microstructure of the sample throughout the gauge section is expected to be reasonably uniform after 50 turns of HPT processing [22,23].

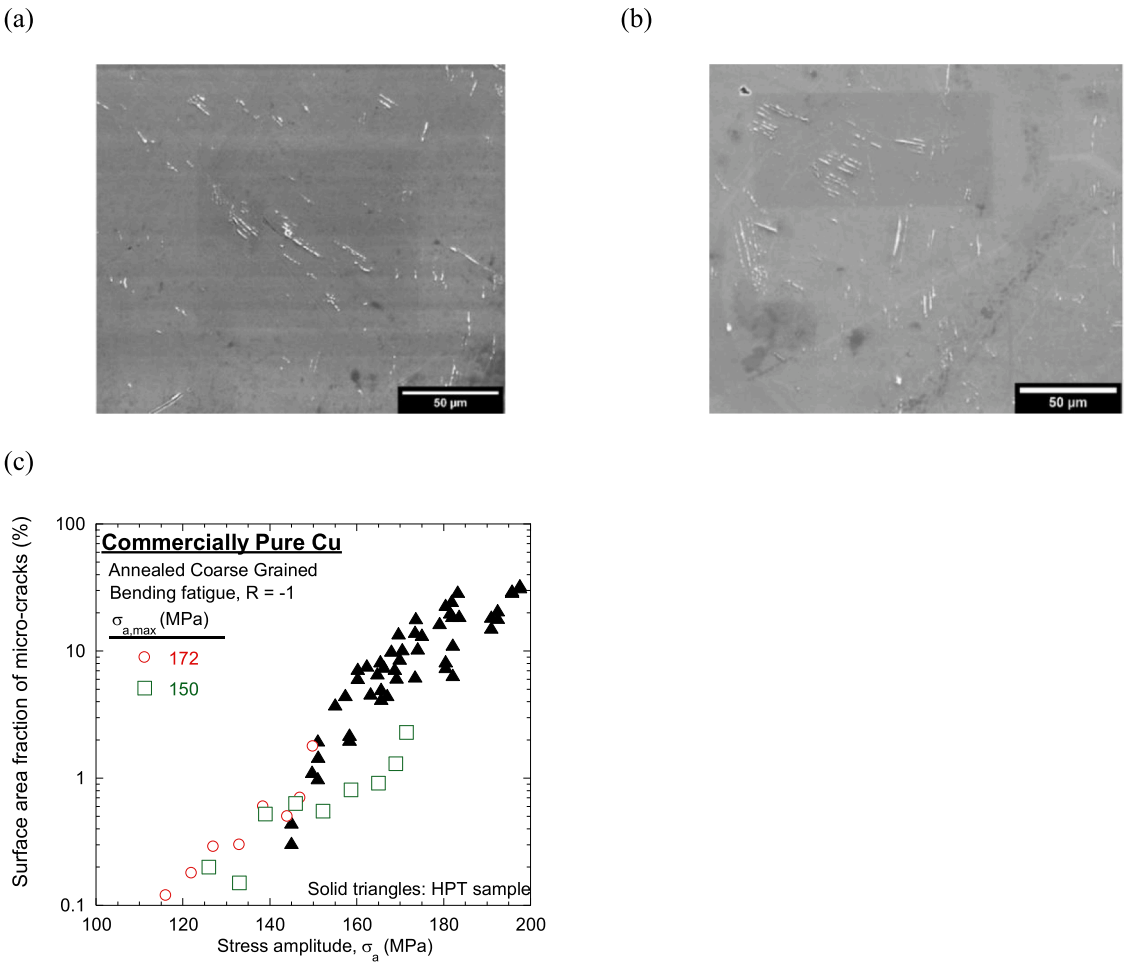

Fig. 5. SEM micrographs of the annealed CG Cu samples following the bending fatigue test performed at $\sigma_{a,\max}$ of (a) 80 and (b) 172 MPa. (c) Variation of the area fraction of the surface micro-cracks as a function of σ_a on a log-log scale. Both flat surfaces of each sample were examined, and an average of both sides was plotted. Data shown in Fig. 3d are also shown here for quick reference.

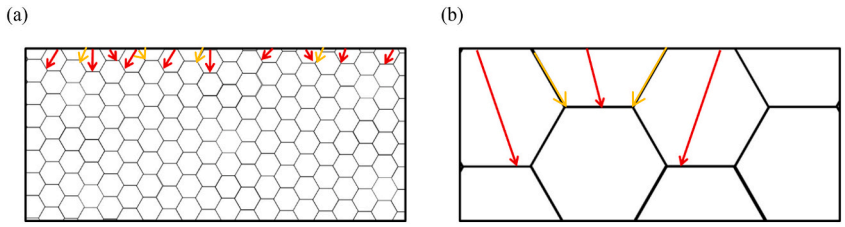

Fig. 6. Schematic illustration of the effect of grain size on the growth of surface micro-cracks under fatigue loading: (a) UFG and (b) CG samples. Arrows represent a few of the micro-cracks originating from the surface. Intragranular cracks are shown in red, while intergranular cracks are shown in yellow. (For interpretation of the references to colour in this figure legend, the reader is referred to the web version of this article.)

studies reporting the total fatigue life [12,14,15]. Overall, it can be concluded that damages in the HPT processed Cu samples were limited to the surface only, and it took longer to generate equivalent damage in the HPT processed samples. This provides a mechanistic explanation for the enhancement in the HCF life of UFG materials.[4]

The origin of fatigue crack nucleation and propagation is extensively studied. Possible crack nucleation sites during fatigue include regions of stress concentrations, inhomogeneities, triple junctions, grain boundaries, shear bands, etc. [34,35] As the grain boundaries may also provide a less tortuous path in a UFG material, it is suggested that intergranular fracture can be prevalent in UFG materials during fatigue [36,37]. In this context, a transition from intragranular to intergranular fracture with a reduction of grain size has also been suggested [38]. On the contrary, only intragranular fracture was reported in UFG Ti [39]. Due to the extensive shear banding in the present study and the size of the shear bands and surface cracks larger than the grain size of UFG Cu, it makes it difficult to analyze and comment on the relative importance of intergranular crack propagation compared to the intragranular crack. Nevertheless, the role of grain boundaries in effectively arresting

[4] The difference between the crack penetration depth into the sample cannot be attributed to the prevalence of large stress gradient (and hence fast drop in the stress across the thickness) in the thinner HPT samples. As a surface micro-crack nucleate and grow, the stress at its tip increases to satisfy the force balance.

intragranular cracks, which is expected to play a significant role in fatigue failure, and hence enhancing the fatigue life of UFG Cu compared to CG Cu is a reasonable assumption.

To further understand the effect of the HPT processing on the formation of dislocation substructure, which is known to control the fatigue life of materials [33,40,41], the thin lamellae of both annealed and HPT samples, fabricated near a region containing a micro-crack within 10 μm depth from the surface, were examined using TEM. Here, firstly, selected area diffraction patterns were obtained (see Fig. 7a). The magnified micrograph shown in Fig. 7a was obtained after tilting the sample along the ZA with $\boldsymbol{g} = (\overline{\mathbf{1}}\,\overline{\mathbf{1}}\,\mathbf{1})$ and it clearly shows the dislocation substructure formed in the annealed sample after a fatigue test. Dislocations were stacked parallel to each other inside the large grains.

Fig. 7b shows the dislocation substructure formed in the HPT sample after fatigue testing. Alike CG Cu samples, dislocations in UFG samples were also confined within the grain in the parallel arrangement. Remarkably, the grain size of the HPT sample remained stable during fatigue loading: the grain size after fatigue testing was ~350 nm as compared to ~300 nm before the test (i.e., following HPT processing). This stability of the grain size during fatigue can be attributed to the low purity of CP Cu and is consistent with a few earlier studies on fatigue of UFG materials [15]. Except for the grain size and hence the distance over which the dislocations were confined, the dislocation substructure formed in the annealed CG and the HPT UFG samples after fatigue were quite similar. Since the initial dislocation substructures in these two types of samples would be very different (e.g., significantly higher dislocation density in the HPT processed samples as compared to the annealed CG sample [1]), one may conclude that difference in the number of cycles taken to reach the same dislocation substructure after fatigue in both types of samples, and hence the fatigue life measured here, was determined by the difference in the initial and the final substructure and the kinetics of its evolution to attain the final configuration.

Although the dislocation substructure shown in Fig. 7 may resemble veins and persistent slip bands (PSBs) that often form during fatigue, further analysis, using much higher magnification micrographs, directional analysis, etc., is required to unambiguously conclude it. However, it should be noted that although PSBs have been observed in polycrystalline Cu, sometimes it is difficult to observe them when the grain size is small [42,43]. Therein, only a distinct wall of dislocations could be observed with moderate spacing [43]. Notably, although extrusion and intrusion at the surface of UFG Cu were observed in an earlier study [43], TEM micrographs of the surface interior did not reveal the formation of PSB.

4. Conclusion

Disks of CP Cu were processed for 50 turns of quasi-constrained HPT at room temperature by applying a compressive pressure of 6 GPa. Both annealed CG and HPT processed UFG samples were cyclically loaded in bending, with R of −1, in the HCF regime until their resonant frequency decreased by 20%. HPT samples took a noticeably larger number of cycles to reach the above failure criterion.

For both CG and UFG Cu samples, the formation of the surface micro-crack depended mainly on the stress amplitude, such that the area fraction of the surface micro-cracks increased with an increase in stress amplitude. In HPT samples, the surface micro-cracks did not form at lower stresses; however, their area fraction was significantly higher than the annealed CG samples at the higher stresses.

Grains of HPT samples did not grow during fatigue loading. Dislocation substructures formed in both the annealed and the HPT samples during fatigue were qualitatively similar. It is speculated that the kinetics of the dislocation substructure evolution in the HPT samples must be significantly slower than that in the annealed CG samples.

As CP Cu processed through a large number of HPT turns shows better HCF life, along with significantly high strength and only a

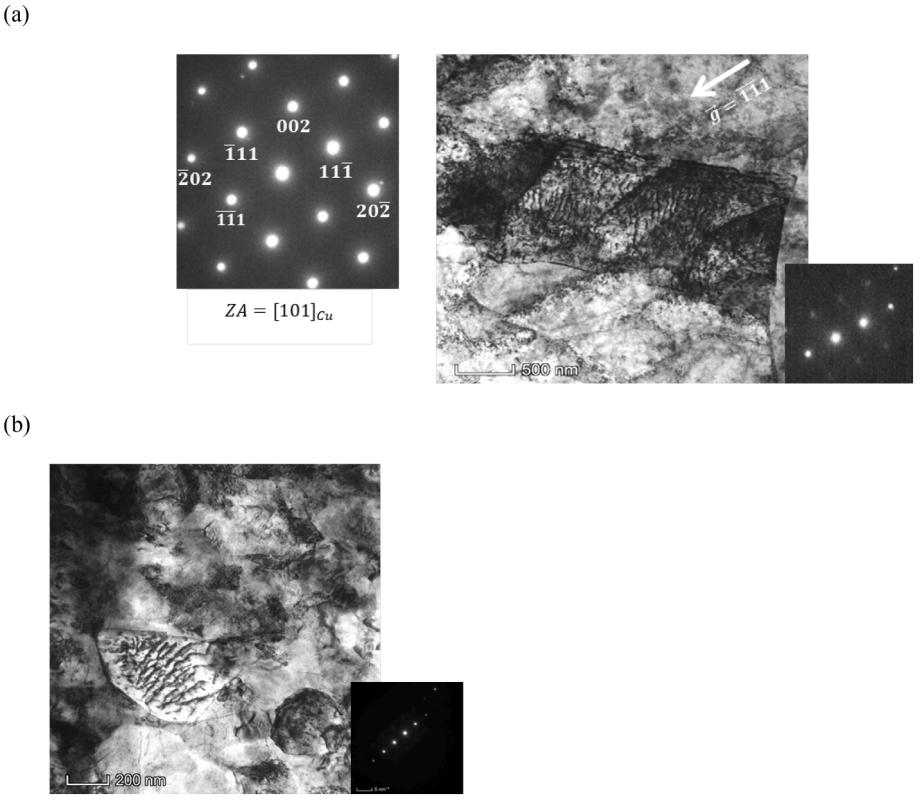

Fig. 7. TEM micrographs showing dislocation arrangement inside a grain of (a) annealed and (b) HPT processed samples after fatigue testing. In (a), a selected area diffraction (SAED) pattern with [101] zone axis is also shown. Here, zone axis, $\vec{g} = (\bar{1}\,\bar{1}\,1)$ was used to obtain the extinction criterion.

moderate loss of electrical conductivity as compared to CG Cu, it appears reasonable to explore the utility of HPT processed Cu for high demanding electrical transmission and connector applications.

Declaration of Competing Interest

The authors declare that they have no known competing financial interests or personal relationships that could have appeared to influence the work reported in this paper.

Acknowledgments

This study was supported in part by the Department of Science and Technology, Ministry of Science and Technology, India, under its National Clean Coal Initiative (AR, SPS and PK), the National Science Foundation of the United States under Grant No. DMR-1810343 (MK and JKH). PK gratefully acknowledges the financial support from DAAD, Germany, which allowed him to travel to Germany on a short-term academic visit.

References

[1] A.P. Zhilyaev, T.G. Langdon, Using high-pressure torsion for metal processing: fundamentals and applications, Prog. Mater. Sci. 53 (2008) 893–979.
[2] R.Z. Valiev, et al., Producing bulk ultrafine-grained materials by severe plastic deformation: ten years later, JOM 68 (2016) 1216–1226.
[3] T.G. Langdon, Twenty-five years of ultrafine-grained materials: achieving exceptional properties through grain refinement, Acta Mater. 61 (2013) 7035–7059.
[4] R.Z. Valiev, T.G. Langdon, Principles of equal-channel angular pressing as a processing tool for grain refinement, Prog. Mater. Sci. 51 (2006) 881–981.
[5] V. Review Segal, Modes and processes of severe plastic deformation (SPD), Materials (Basel). 11 (2018) 1175.
[6] R.Z. Valiev, I.V. Alexandrov, Y.T. Zhu, T.C. Lowe, Paradox of Strength and Ductility in Metals Processed Bysevere Plastic Deformation, cambridge.org vol. 17, 2014, pp. 5–8.
[7] I.A. Ovid'ko, R.Z. Valiev, Y.T. Zhu, Review on superior strength and enhanced ductility of metallic nanomaterials, Prog. Mater. Sci. 94 (2018) 462–540.
[8] T. Mungole, P. Kumar, M. Kawasaki, T.G. Langdon, The contribution of grain boundary sliding in tensile deformation of an ultrafine-grained aluminum alloy having high strength and high ductility, J. Mater. Sci. 50 (2015) 3549–3561.
[9] T. Mungole, P. Kumar, M. Kawasaki, T.G. Langdon, A critical examination of the paradox of strength and ductility in ultrafine-grained metals, J. Mater. Res. 29 (2014) 2534–2546.
[10] Y. Wang, M. Chen, F. Zhou, E. Ma, High tensile ductility in a nanostructured metal, Nature 419 (2002) 912–915.
[11] H.-K. Kim, M.-I. Choi, C.-S. Chung, D.H. Shin, Fatigue properties of ultrafine grained low carbon steel produced by equal channel angular pressing, Mater. Sci. Eng. A 340 (2003) 243–250.
[12] H.W. Höppel, et al., An overview: fatigue behaviour of ultrafine-grained metals and alloys, Int. J. Fatigue 28 (2006) 1001–1010.
[13] H. Mughrabi, H.W. Höppel, M. Kautz, Fatigue and microstructure of ultrafine-grained metals produced by severe plastic deformation, Scr. Mater. 51 (2004) 807–812.
[14] A. Vinogradov, S. Hashimoto, Multiscale phenomena in fatigue of ultra-fine grain materials - an overview, Mater. Trans. 42 (2001) 74–84.
[15] G. Khatibi, J. Horky, B. Weiss, M.J. Zehetbauer, High cycle fatigue behaviour of copper deformed by high pressure torsion, Int. J. Fatigue 32 (2010) 269–278.
[16] H.W. Höppel, R.Z. Valiev, On the possabilities to enhance the fatigue properties of ultrafine-grained metals, Z. Met. 93 (2002) 641–648.
[17] Z. Zhang, et al., Effects of Dislocation Slip Mode on High-Cycle Fatigue Behaviors of Ultrafine-Grained Cu–Zn alloy Processed by Equal-Channel Angular Pressing, Elsevier, 2022.
[18] X.H. An, S.D. Wu, Z.G. Wang, Z.F. Zhang, Significance of stacking fault energy in bulk nanostructured materials: insights from cu and its binary alloys as model systems, Prog. Mater. Sci. 101 (2019) 1–45.
[19] X.H. An, Q.Y. Lin, S.D. Wu, Z.F. Zhang, Mechanically driven annealing twinning induced by cyclic deformation in nanocrystalline cu, Scr. Mater. 68 (2013) 988–991.
[20] X.H. An, S.D. Wu, Z.G. Wang, Z.F. Zhang, Enhanced cyclic deformation responses of ultrafine-grained Cu and nanocrystalline Cu–Al alloys, Acta Mater. 74 (2014) 200–214.
[21] X. An, Q. Lin, S. Wu, Z. Zhang, Improved fatigue strengths of nanocrystalline Cu and Cu-Al alloys, Mater. Res. Lett. 3 (2015) 135–141.
[22] A. Rijal, S.P. Singh, J.-K. Han, M. Kawasaki, P. Kumar, Effect of high-pressure torsion on hardness and electrical resistivity of commercially pure Cu, Adv. Eng. Mater. 22 (2020) 1900547.
[23] A. Rijal, S.P. Singh, J.K. Han, M. Kawasaki, P. Kumar, Effect of HPT processing followed by long term natural ageing on mechanical and electrical properties of commercially pure Cu, Lett. Mater. 9 (2019) 561–565.
[24] A.P. Zhilyaev, I. Shakhova, A. Belyakov, R. Kaibyshev, T.G. Langdon, Effect of annealing on wear resistance and electroconductivity of copper processed by high-pressure torsion, J. Mater. Sci. 49 (2014) 2270–2278.
[25] K. Edalati, K. Imamura, T. Kiss, Z. Horita, Equal-Channel Angular Pressing and High-Pressure Torsion of Pure Copper: Evolution of Electrical Conductivity and Hardness with Strain, jstage.jst.go.jp, 2011, https://doi.org/10.2320/matertrans.MD201109.
[26] R.B. Figueiredo, P.H.R. Pereira, M.T.P. Aguilar, P.R. Cetlin, T.G. Langdon, Using finite element modeling to examine the temperature distribution in quasi-constrained high-pressure torsion, Acta Mater. 60 (2012) 3190–3198.
[27] T. Straub, M.F. Berwind, T. Kennerknecht, Y. Lapusta, C. Eberl, Small-scale multiaxial setup for damage detection into the very high cycle fatigue regime, Exp. Mech. 55 (2015) 1285–1299.
[28] A. Mishra, et al., High-strain-rate response of ultra-fine-grained copper, Acta Mater. 56 (2008) 2770–2783.
[29] J.L. Jordan, C.R. Siviour, G. Sunny, C. Bramlette, J.E. Spowart, Strain Rate-Dependant Mechanical Properties of OFHC Copper, 2022, https://doi.org/10.1007/s10853-013-7529-9.
[30] S.R. Agnew, A.Y. Vinogradov, S. Hashimoto, J.R. Weertman, Overview of fatigue performance of Cu processed by severe plastic deformation, J. Electron. Mater. 28 (1999) 1038–1044.
[31] C. Xu, et al., Fatigue behavior and damage characteristic of ultra-fine grain low-purity copper processed by equal-channel angular pressing (ECAP), Mater. Sci. Eng. A 475 (2008) 249–256.
[32] P. Lukáš, L. Kunz, L. Navrátilová, O. Bokůvka, Fatigue damage of ultrafine-grain copper in very-high cycle fatigue region, Mater. Sci. Eng. A 528 (2011) 7036–7040.
[33] S. Suresh, Fatigue of Materials, 1998.
[34] M. Goto, et al., Crack initiation mechanism in ultrafine-grained copper fabricated by severe plastic deformation in the high-cycle fatigue regime, Mater. Sci. Eng. A 788 (2020), 139569.
[35] S.D. Wu, et al., Shear bands in cyclically deformed ultrafine grained copper processed by ECAP, Mater. Sci. Eng. A 387–389 (2004) 560–564.
[36] A. Vinogradov, Fatigue limit and crack growth in ultra-fine grain metals produced by severe plastic deformation, J. Mater. Sci. 42 (2007) 1797–1808.
[37] Y. Estrin, A. Vinogradov, Fatigue behaviour of light alloys with ultrafine grain structure produced by severe plastic deformation: an overview, Int. J. Fatigue 32 (2010) 898–907.
[38] A. Hohenwarter, R. Pippan, Fracture and fracture toughness of nanopolycrystalline metals produced by severe plastic deformation, Philos. Trans. R. Soc. A Math. Phys. Eng. Sci. 373 (2015).
[39] S. Fintová, M. Arzaghi, I. Kuběna, L. Kunz, C. Sarrazin-Baudoux, Fatigue crack propagation in UFG Ti grade 4 processed by severe plastic deformation, Int. J. Fatigue 98 (2017) 187–194.
[40] N.Y. Jin, A.T. Winter, Dislocation structures in cyclically deformed [001] copper crystals, Acta Metall. 32 (1984) 1173–1176.
[41] N.Y. Jin, Dislocation structures in cyclically deformed [oil] copper crystals, Philos. Mag. Lett. 56 (1987) 23–28.
[42] C.D. Liu, M.N. Bassim, D.X. You, Dislocation structures in fatigued polycrystalline copper, Acta Metall. Mater. 42 (1994) 3695–3704.
[43] S.R. Agnew, J.R. Weertman, Cyclic softening of ultrafine grain copper, Mater. Sci. Eng. A 244 (1998) 145–153.
[44] H.W. Hoppel, Z.M. Zhou, H. Mughrabi, R.Z. Valiev, Microstructural study of the parameters governing coarsening and cyclic softening in fatigued ultrafinegrained copper, Philos. Mag. A Phys. Condens. Matter, Struct. Defects Mech. Prop. 82 (2002) 1781–1794.